Thermodynamic assessment of two-step nucleation occurrence in supercritical fluid

Pierre Guillou, Samuel Marre, Arnaud Erriguible

The Journal of Supercritical Fluids 211 (2024) 106292

Contents lists available at ScienceDirect

The Journal of Supercritical Fluids

journal homepage: www.elsevier.com/locate/supflu

Thermodynamic assessment of two-step nucleation occurrence in supercritical fluid

P. Guillou [a,b], S. Marre [b], A. Erriguible [a,b,*]

[a] CNRS, Univ. Bordeaux, Bordeaux INP, I2M, UMR 5295, Pessac Cedex 33600, France
[b] CNRS, Univ. Bordeaux, Bordeaux INP, ICMCB, UMR 5026, Pessac Cedex 33600, France

HIGHLIGHTS

- Thermodynamical evaluation of the two-step nucleation with PREOS.
- Liquid droplets can precipitate at low supersaturation instead of solid particles.
- The spinodal limits lie at higher supersaturation.
- The metastable liquid phase composition depends slightly on the pressure.

GRAPHICAL ABSTRACT

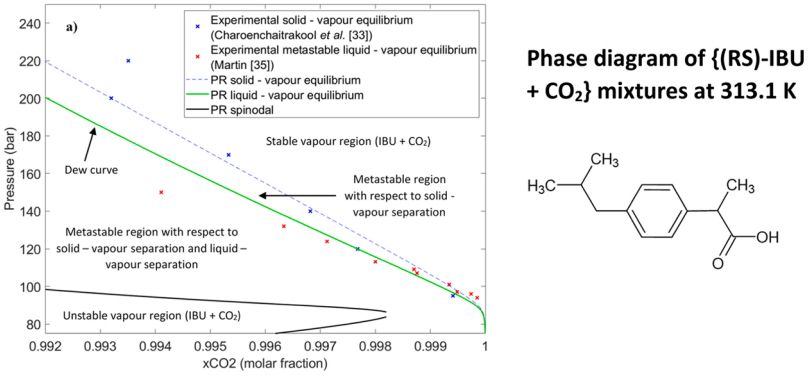

ARTICLE INFO

Keywords:
Two-step nucleation
Crystallization
PREOS
Supercritical CO2
Spinodal decomposition

ABSTRACT

For the crystallization of an API in supercritical CO_2, a two – step nucleation mechanism involves the apparition of metastable liquid droplets in the vapour phase composed of the API dissolved in the CO_2, before crystallization. To find out the pressure and temperature conditions such a two – step mechanism could be observed, we studied the stability / metastability / instability for {(S)-Naproxen + CO_2} and {(RS)-Ibuprofen + CO_2} vapour binary mixtures. Thermodynamic computations proposed in the paper, have shown that a mixture of API and CO_2 at elevated pressures can be unstable and/or metastable with respect to a liquid-vapour equilibrium and at the same time with respect to a solid-vapour equilibrium. Depending on the degree of supersaturation, such a mixture can potentially first decompose via spinodal decomposition into coexisting liquid and vapour phases, which turn due to nucleation and growth theory to a solid-fluid equilibrium.

1. Introduction

About 40 % of the marketed and 90 % of the drugs under development present low water solubility, resulting in low bioavailability, unsatisfactory therapeutic efficiency and high attrition rates [1]. There are two main strategies for improving the pharmacokinetics of these molecules without sophisticated formulations. The first one is submicronization that allows the surface to volume ratio of the particles to

* Corresponding author at: CNRS, Univ. Bordeaux, Bordeaux INP, I2M, UMR 5295, Pessac Cedex 33600, France.
E-mail address: erriguible@enscbp.fr (A. Erriguible).

https://doi.org/10.1016/j.supflu.2024.106292
Received 22 February 2024; Received in revised form 18 April 2024; Accepted 24 April 2024
Available online 27 April 2024

be drastically increased. The second one is the control of crystallinity. Indeed, amorphous materials, which are characterized by the absence of long-range molecular order, offer improved apparent solubility and dissolution rates with respect to crystalline drugs, due to the lower energy barrier required to dissolve the particles. However, they suffer from thermodynamic instability and crystallization tendencies through aging processes and storage [2,3]. Therefore, controlling both the size and crystallinity is very challenging, while it is an absolute requirement for applications in the pharmaceutical field.

Regarding the reduction of particle size, recent studies of our team [4] demonstrated that a combination of supercritical fluids and microfluidic reactors (μSAS) can significantly improve the performance and reproducibility of antisolvent processes. Specifically, supercritical CO_2 was used for its mild critical conditions of temperature and pressure well adapted to fragile organic molecules and for its non-reactive characteristics. We highlighted the high performance of the microreactor working in turbulent conditions, resulting in ultra-fast mixing times (10^{-4} - 10^{-5} s) [5] and organic nanoparticles (NPs) with unprecedented average diameter down to 15 nm. These results underline the value of this technique for the controlled production of very small organic NPs, and potentially pave the way for practical applications involving the processing of a large number of organic compounds. So far, the amorphous/crystalline phase control using this technique has not been studied. The appearance of amorphous or crystalline phase depends on the supersaturation levels, so, a media like supercritical fluids, for which conditions can be easily tuned permits to reach a large window of supersaturation levels.

According to the classical nucleation theory, the supersaturation of a solute in a mother solution leads to the formation of nuclei, which will keep the same crystalline form throughout the process. It is assumed that the two order parameters governing classical nucleation phenomena, ordering and densification, occur simultaneously. In the non-classical theory, the densification step, leading to an "amorphous or dense liquid" phase, occurs prior to the ordering of the molecules, leading to the crystalline phase. Many studies in the literature postulate that the first step is due to spinodal decomposition of the mother solution due to high levels of supersaturation [6,7]. These conditions of high supersaturation levels are often encountered in supercritical precipitation processes.

Since the pioneering work of Wolde and Frenkel [8] on the demonstration of two-step protein nucleation by numerical simulation, the community has been interested in this phenomenon for the precipitation of organic (e.g. proteins [9]) and inorganic (mineral) materials. To date, the literature offers serious studies, mainly based on in situ experiments, to study this particular nucleation pathway. A consensus is now emerging to rule that the classical nucleation theory is not the only pathway to nucleation. Recent works proposed the demonstration of two-stage nucleation for different media, including liquid-solid, solid--solid and vapour-solid [9].

In this paper, we focus on the precipitation of organic materials from a compressed fluid mixture. To our knowledge, there is no study of the two-step nucleation phenomenon in such a medium. Given the properties of the supercritical fluid, between liquid (“high” density) and gas (low viscosity), the behaviour of the phenomenon could be close to that of precipitation in a vapour medium, for which the appearance of a liquid phase has been observed in most studies [9]. In addition, several works highlight the appearance of a dense liquid phase, rather stable given its viscosity, in the case of the precipitation of organic materials [10], certainly resulting from spinodal decompositions or liquid/liquid separations. Wiedenbeck *et al.* [11] proposed to manage the appearance of the amorphous or crystalline phase by playing with the appearance of the liquid phase depending on the environmental conditions of precipitation. Very recently, Zhang *et al.* [12] proposed a CALPHAD thermodynamic model of oiling-out coupled with microfluidic observations of the precipitation of poorly water-soluble organic compounds when water is added as an antisolvent. The authors demonstrated the appearance of a metastable liquid phase in the bulk liquid phase, before or instead of the expected crystallization.

In this context, we intend to open up a new route for processing amorphous or crystalline particles using supercritical processes. To do so, we first need to analyse in depth, from a thermodynamic point of view, the conditions under which two-step nucleation can occur from CO_2-rich fluid mixtures at elevated pressure. In this paper, we propose a thermodynamic study of a mixture composed of an API solute and compressed CO_2, (S)-Naproxen (NPX) + carbon dioxide (CO_2) and (RS)-Ibuprofen (IBU) + carbon dioxide (CO_2), in order to determine the stable limits (solid/vapour separation), the metastable limits (liquid/vapour separation) and the unstable limits, *i.e.* spinodal decomposition. Finally, we rationalize the probability of occurrence of a two-step nucleation by estimating the supersaturation ratio, required to reach the metastability and instability limits.

2. Numerical modeling

2.1. Determination of the stable and metastable limits

The Peng – Robinson [13] Equation of State (Eq. (1)), a well-known cubic equation of state, has been chosen to describe both vapour and liquid phases and along with supercritical fluids phase for single compounds or mixtures, it reads as:

$$P = \frac{NRT}{V - Nb_m} - \frac{a_m N^2}{(V - Nb_m m_1)(V - Nb_m m_2)} \tag{1}$$

$$m_1 = -1 + \sqrt{2} \tag{2}$$

$$m_2 = -1 - \sqrt{2} \tag{3}$$

For each compound i:

$$a_i = 0.45724 \frac{R^2 T_{c,i}^2}{P_{c,i}} \tag{4}$$

$$b_i = 0.07780 \frac{R T_{c,i}}{P_{c,i}} \tag{5}$$

$$\alpha_i = \left[1 + \kappa_i \left(1 - T_{r,i}^{0.5}\right)\right]^2 \tag{6}$$

$$T_{r,i} = \frac{T}{T_{c,i}} \tag{7}$$

$$\kappa_i = \left(0.37464 + 1.54226\omega_i - 0.26992\omega_i^2\right) \tag{8}$$

The Van der Walls mixing rule is chosen for its ease of application and relatively good accuracy:

$$a_m = \sum_i \sum_j x_i x_j (a\alpha)_{ij} \tag{9}$$

$$b_m = \sum_i x_i b_i \tag{10}$$

$$(a\alpha)_{ij} = \left(1 - k_{ij}\right)\sqrt{(a_i \alpha_i)\left(a_j \alpha_j\right)} \tag{11}$$

$$k_{ij} = k_{ji} \tag{12}$$

$$k_{ii} = 0 \tag{13}$$

with k_{ij} the binary interaction parameters. The physical properties of all the components studied in this paper are reported in appendix, Table A.1.

The liquid-vapour equilibria are calculated in a classical way, using chemical potentials through the use of fugacities. So, the equilibria compositions are deduced from the equality of the component fugacities

in each phase. The calculation of the fugacity coefficient φ_i of the compound i in the liquid or vapour phase using Eq. (14) leads to the fugacity f_i (Eq. (15)):

$$\ln(\varphi_i) = \frac{b_i}{b_m}(Z-1) - \ln(Z-B) - \frac{A}{2\sqrt{2}B}\left(\frac{2}{a_m}\sum_j x_j(a\alpha)_{ij} - \frac{b_i}{b_m}\right) \ln\left[\frac{Z+(1+\sqrt{2})B}{Z+(1-\sqrt{2})B}\right] \quad (14)$$

$$f_i = \varphi_i x_i P \quad (15)$$

The solubility of the compound i of interest is defined as the molar fraction x_i dissolved in the fluid phase at the fluid – solid equilibrium. For the considered binary systems, the API pure solid phase sublimates in a supercritical vapour-like phase enriched in CO_2, so that calculating the solubility of the API is equivalent to calculate the molar fraction x_i of the API in the supercritical vapour-like phase at the solid – fluid equilibrium. For the sake of simplicity, the solid – supercritical vapour-like fluid equilibrium will hereafter be referred to as solid – vapour equilibrium. In this paper, we have compared two classical ways of modeling the fugacity f_i^S of compound i in the solid phase.

First, the "Subcooled – liquid approximation" has been developed by De Swaan Arons and Diepen [14], then detailed by Prausnitz *et al.* [15] at moderate pressures with an incompressible liquid phase, and Kikic *et al.* [16] and Seiler *et al.* [17] at higher pressures: the pure solid phase is considered as a pure subcooled liquid phase, the fugacity is then adjusted using melting properties and some volumetric data relative to compound i. As suggested by Kikic *et al.* [16], the pressure term in the exponential factor in Eq. (16) can be neglected since the difference between the pure solid and liquid molar volumes is usually negligible. So, the solid fugacity can be described by the following relation:

$$f_i^{S,pure}(T,P) \approx f_i^{L,pure}(T,P)\exp\left[\frac{\Delta H_{m,i}}{RT_{m,i}}\left(1-\frac{T_{m,i}}{T}\right) + \int_{P_0}^{P}\left(\frac{v_i^S - v_i^L}{RT}\right)dP\right] \approx \varphi_i^{L,pure}(T,P)P\exp\left[\frac{\Delta H_{m,i}}{RT_{m,i}}\left(1-\frac{T_{m,i}}{T}\right)\right] \quad (16)$$

Secondly, we tested the "Sublimation pressure estimation" detailed by Tester and Modell [18]. For that, we used the Lee – Kesler Eq. (18) [19], assuming that the fugacity coefficient of compound i in the vapour above pure solide phase i at its sublimation pressure at temperature T is close to unity. Consequently, the solid fugacity can be estimated by the following relations:

$$f_i^S(T,P) = P_{sub,i}\varphi_i^V(T,P_{sub,i})\exp\left[\frac{v_i^S(P-P_{sub,i})}{RT}\right] \approx P_{sub,i}\exp\left[\frac{v_i^S(P-P_{sub,i})}{RT}\right] \quad (17)$$

Where the sublimation pressure $P_{sub,i}$ is given by:

$$\ln\left(\frac{P_{sub,i}}{P_{c,i}}\right) = A_1 + \frac{A_2}{T_{r,i}} + A_3\ln(T_{r,i}) + A_4T_{r,i}^6 + \omega_i\left(B_1 + \frac{B_2}{T_{r,i}} + B_3\ln(T_{r,i}) + B_4T_{r,i}^6\right) \quad (18)$$

Two sets of LK parameters have been compared (Table A.2). The first one ($LK^{original}$) is the original set of Lee and Kesler [19] and the second (LK^{B3}) was proposed by Wang and Hsieh [20], which may provide more accuracy on the sublimation pressure estimation in some cases.

The main advantage in using the sublimation pressure estimation is that it does not require the knowledge of the melting characteristics of the solid, which can be experimentally challenging to obtain. On the other hand, it requires the knowledge of the pure solid molar volume v_i^S.

From a numerical point of view, all calculations for phase equilibria have been performed using an open source Matlab code published by Martin *et al.* [21]. The code is well documented, easy to use and modify. Numerical algorithms are derived from Walas [22] or Gupta *et al.* [23]. For the liquid – vapour equilibria estimation, the standard bubble point algorithm, the standard dew point algorithm, the isothermal flash multi-component Rashford – Rice algorithm, and the isothermal multi-component multiphase equilibrium flash based on minimization of Gibbs free energy are available. For the solid – vapour equilibria, the isothermal multi-component multiphase equilibrium flash based on minimization of Gibbs free energy has been used.

For the k_{ij} parameters estimation, at a given temperature T, the Absolute Average Relative Deviation (ARRD) between the experimental data of API solid solubilities and the numerical ones, $AARD = \sum_{i=1}^{n_{exp}}\left|\frac{x_{API}^{exp} - x_{API}^{model}}{x_{API}^{exp}}\right|$, has been minimized.

2.2. Determination of the unstable limits

The spinodal limit is classically defined as the limit of stability, where no nucleation energy barrier has to be overcome: the phase change then occurs spontaneously. For our binary mixtures {API + CO_2}, the vapour single phased initial mixture decomposes spontaneously into 2 phases: the first is a vapour-like phase enriched in CO_2 and the second is a liquid-like phase enriched in API. This transformation is called a "spinodal decomposition", described by the Cahn-Hilliard formalism [24,25], different from the Classical Nucleation Theory (CNT), describing nucleation in the metastable domain.

As detailed by Tester and Modell [18], in the case of a single compound, the spinodal limits can easily be calculated by estimating the (P, V) couple ensuring Eq. (19) at a given temperature T. This is done by solving Eq. (20), which represents the analytical derivative of pressure with respect to volume, using PREOS:

$$\left(\frac{\partial P}{\partial V}\right)_{T,N} = 0 \quad (19)$$

$$-\frac{NRT}{(V-Nb_m)^2} + \frac{a_mN^2}{(V-Nb_mm_1)(V-Nb_mm_2)^2} + \frac{a_mN^2}{(V-Nb_mm_1)^2(V-Nb_mm_2)} = 0 \quad (20)$$

However, the estimation of the spinodal limits is much more complicated in the case of mixtures. As shown by Heidemann and Khalil [26] and Aursand *et al.* [27], a formalism based on the Helmholtz free energy A is well adapted for PREOS using a (T, V, **N**) approach. Heidemann and Khalil [26] calculated the spinodal limit on calculating determinants of Hessian matrices, whereas Aursand *et al.* [27] used a mathematically equivalent approach based on the eigenvalues of Hessian composition matrices. We chose the Aursand's approach because it provides, to our opinion, an easiest and interesting geometrical interpretation of the spinodal limits. Characterizing the stability of a given single phase mixture is equivalent to evaluate the local curvature of its Helmholtz free energy A. It is evaluated calculating the eigenvalues of the Hessian composition matrix of A for each composition. When all the eigenvalues are positive, the Helmholtz free energy is locally a convex surface, so that the mixture is thermodynamically considered as stable.

When all the eigenvalues are negative, the Helmholtz free energy is locally a concave surface, so that the mixture is thermodynamically considered as unstable. Finally, when at least one eigenvalue is negative, we have locally a saddle point, so that the mixture is also thermodynamically considered as unstable. The saddle points represent the spinodal limits.

2.2.1. Numerical procedure

By considering the Peng – Robinson [13] equation of state, we worked directly on analytical expressions of the derivatives of 2nd order of the Helmholtz free energy A, instead of using fugacities. The method used in this paper is summarised below, looking for the saddle points in the composition space (the theoretical and mathematical details are described in [27]).

When coming from a stable domain to an unstable domain, the original stability criteria, at fixed (T, V, **N**), is given by:

$$\min\{eig(\nabla_{V,\boldsymbol{N}}\nabla_{V,\boldsymbol{N}}A(T,V,\boldsymbol{N}))\} \geq 0 \tag{21}$$

From a mathematical point of view, only the study of the matrix Φ, part of the Hessian matrix of A relative to the molar quantities, is necessary. The spinodal limit is then found when the smallest eigenvalue of Φ becomes zero, which means that we cross the spinodal limit at a local saddle point:

$$\Phi = \nabla_{\boldsymbol{N}}\nabla_{\boldsymbol{N}}A(T,V,\boldsymbol{N}) \tag{22}$$

$$\min\{eig(\Phi)\} = 0 \tag{23}$$

For binary mixtures, the Hessian matrix Φ is given by:

$$\Phi(T,V,\boldsymbol{N}) = \begin{bmatrix} \dfrac{\partial^2 A}{\partial N_1^2} & \dfrac{\partial^2 A}{\partial N_1 . \partial N_2} \\ \dfrac{\partial^2 A}{\partial N_2 . \partial N_1} & \dfrac{\partial^2 A}{\partial N_2^2} \end{bmatrix} \tag{24}$$

The Φ matrix has to be decomposed into its ideal and excess parts according to:

$$A(T,V,\boldsymbol{N}) = A_{ideal}(T,V,\boldsymbol{N}) + A_{excess}(T,V,\boldsymbol{N}) \tag{25}$$

$$\Phi = \Phi_{ideal} + \Phi_{excess} \tag{26}$$

The necessary 2nd order derivatives of the ideal part Φ_{ideal} are deduced from the following relations:

$$\left.\frac{\partial A_{ideal}}{\partial N_i}\right)_{T,V,N_{j\neq i}} = \mu_i^0(T) + RT\ln\left(\frac{N_i RT}{VP^0}\right) \tag{27}$$

$$\left.\frac{\partial^2 A_{ideal}}{\partial N_i^2}\right)_{T,V,N_{j\neq i}} = \frac{RT}{N_i} \tag{28}$$

$$\left.\frac{\partial^2 A_{ideal}}{\partial N_i \ \partial N_j}\right)_{T,V} = 0 \tag{29}$$

For an ease of resolution, the ideal part Φ_{ideal} of the Hessian matrix is then normalized [27,28] at a fixed composition $\overline{\boldsymbol{N}}$ and temperature T to make the ideal part of the Hessian matrix equal to the identity matrix $\bar{\bar{I}}$. For that, we introduced the variables ε_i defined as follows:

$$\varepsilon_i = \sqrt{\frac{RT}{\overline{N_i}}}(N_i - \overline{N_i}) \tag{30}$$

$$N_i = \overline{N_i} + \varepsilon_i\sqrt{\frac{\overline{N_i}}{RT}} \tag{31}$$

$$\left.\frac{\partial^2 A_{ideal}}{\partial \varepsilon_i^2}\right)_{T,V,\varepsilon=0} = \frac{\overline{N_i}}{N_i} = 1 \tag{32}$$

$$\left.\frac{\partial^2 A_{ideal}}{\partial \varepsilon_i \partial \varepsilon_j}\right)_{T,V,\varepsilon=0} = 0 \tag{33}$$

The 2nd order derivatives of the excess part Φ_{excess} are calculated using PREOS:

$$A_{excess}(T,V,\boldsymbol{N}) = \int_V^{+\infty}\left(P - \frac{NRT}{V}\right)dV \tag{34}$$

$$A_{excess}(T,V,\boldsymbol{N}) = \int_V^{+\infty}\left(\frac{NRT}{V - Nb_m} - \frac{a_m N^2}{(V - Nb_m m_1)(V - Nb_m m_2)} - \frac{NRT}{V}\right)dV \tag{35}$$

$$A_{excess}(T,V,\boldsymbol{N}) = NRT\ln\left(\frac{V}{V - Nb_m}\right) - \frac{a_m N}{b_m(m_1 - m_2)} \ln\left(\frac{V - Nb_m m_2}{V - Nb_m m_1}\right) \tag{36}$$

Considering the previous developments, at the given composition of the mixture $\overline{\boldsymbol{N}}$, the Hessian matrix is finally defined by:

$$\Phi(\overline{\boldsymbol{N}}) = \Phi_{\varepsilon=0} = \bar{\bar{I}} + \Phi_{excess,\varepsilon=0} \tag{37}$$

It is then possible to easily visualize the spinodal line in the (V_m, T) space at the intersection of the zero plan and the $\min\{eig(\Phi)\}$ surface, as represented for example in Fig. 1, for a {(S)-NPX + CO_2} mixture (x_{CO2} = 0.65).

This type of representation is very useful to initialize the following algorithm, to find the couples (V_m, T) all along the spinodal line, and then the pressure, at a given composition $\overline{\boldsymbol{N}}$. The calculation algorithm is as follow:

Step1: V_m and composition $\overline{\boldsymbol{N}}$ are given, calculate Φ when varying T around an initial well chosen temperature T_0

Step 2: find numerically T with $\min\{eig(\Phi)\} = 0$ for the saddle point

Step 3: calculate P using PREOS

Step 4: slightly modify V_m at $\overline{\boldsymbol{N}}$ and use the previous temperature T to initialize the new temperature research, then go to step 2

3. Validation

While equilibrium calculations are rather classical in solid – vapour or liquid – vapour supercritical conditions, spinodal calculations are far

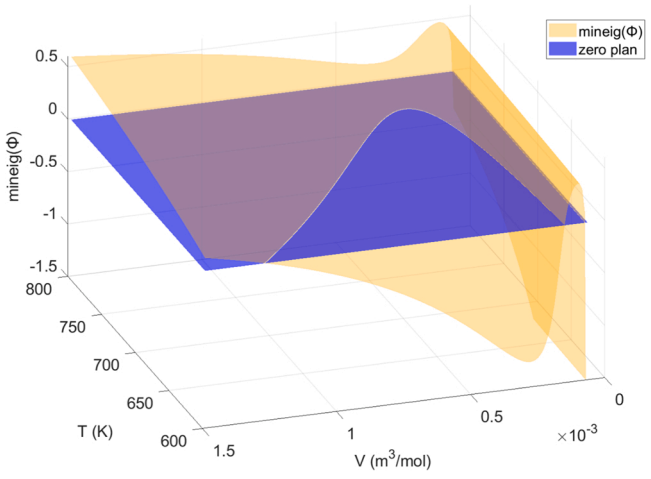

Fig. 1. Spinodal limit visualization in the (V_m, T) space for a {(S)-NPX + CO_2} mixture (x_{CO2} = 0.65).

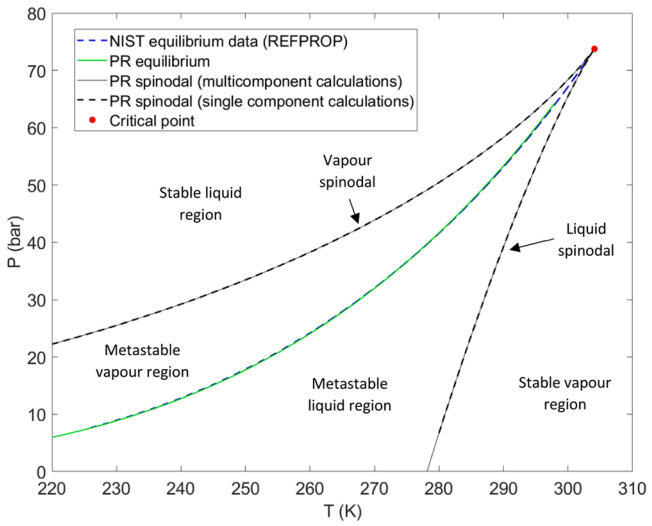

Fig. 2. CO_2 (P, T) diagram.

less common. We present in this part two validation cases to compare our calculations with literature results.

3.1. Test case 1: the single component CO_2

We first tested our multicomponent spinodal calculations on pure CO_2 to compare with the classical single component spinodal calculations usually used for pure components (Eqs. (19) and (20)).

We present our (P, T) results in Fig. 2.

We note that the multicomponent calculations are consistent with single component calculations, since the two methods give exactly the same results. As expected, the critical point lies at the top of the spinodal curve in the (P, T) diagram. The equilibrium curve is more difficult to calculate when approaching the critical point because of classical convergence problems, but due to the shape of the curve, we can assume that it merges with the spinodal curve at the critical point as expected.

Physically, when coming from the stable liquid domain on the left of the diagram, it is possible to cross the equilibrium line without vaporization, the liquid phase becomes metastable. Then, when crossing the liquid spinodal, the liquid phase becomes intrinsically unstable and suddenly vaporizes. The inverse phenomenon can also occur, the condensation, with the vapour phase (starting from the right side of the diagram) crossing successively the equilibrium line and the vapour spinodal.

3.2. Test case 2: mixture with 5 components

We then tested our modeling on a 5 components mixture already studied by Aursand et *al.* [27], which composition is given in Table 1. The spinodal limits and the liquid – vapour equilibria are represented in a (P, T) diagram in Fig. 3. The interaction parameters k_{ij} are chosen to be equal to 0.

As for pure CO_2, the equilibrium curves become difficult to calculate when approaching some points, particularly the critical point located close to (245 K, 96 bar) according to Aursand *et al.* [27], but due to the shape of the global curve, we can assume that they merge with the spinodal limits at the critical point. Compared to the work of Aursand *et al.* [27], we found similar overall results for both the equilibrium and the spinodal limits, except for the vapour spinodal curve below approximatively 40 bar. It's probably due to the fact that Aursand *et al.* [27] has carried out his calculations using GERG2008EOS instead of PREOS.

Table 1
Composition of the 5 components mixture studied by Aursand et al. [27].

	Methane CH_4	Ethane C_2H6	Propane C_3	n-butane C_4H_{10}	Nitrogen N_2
Molar fraction	0.75	0.10	0.07	0.03	0.05

Table 2
PREOS k_{ij} and AARD on solubility for (S)-NPX at 313.1 K.

Subcooled liquid method		Lee – Kesler equation	
k_{ij}	AARD (%)	k_{ij}	AARD (%)
0.14399	11.5	0.24598 ($LK^{original}$) 0.16286 (LK^{B3})	20.7 ($LK^{original}$) 7.5 (LK^{B3})

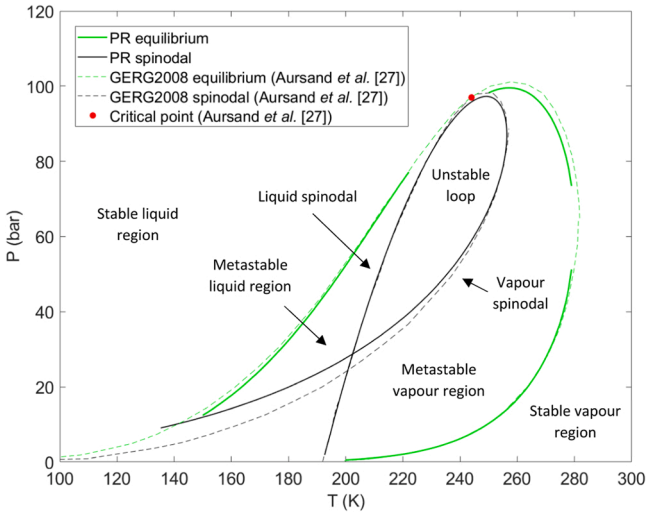

Fig. 3. Spinodal limits and equilibria of the 5 components mixture studied by Aursand et al. [27], (P, T) diagram.

Physically, as for the previous single component case, the diagram shows the existence of two metastable domains where respectively the liquid phase and the vapour phase could be observed. In contrast, an unstable loop is highlighted, where the single phased mixture is intrinsically unstable: it decomposes into two phases with different compositions by "spinodal decomposition". The mechanism of this demixtion is fundamentally different from the mechanism described by the Classical Nucleation Theory.

4. Results and discussion

In this section, we have chosen to study two API model organic components, largely studied in the supercritical community [29], for which solubility data and/or triple-points data (SLV-lines = Solid – Liquid – Vapour lines) in compressed CO_2 are available: the (S)-Naproxen [30–32] and the (RS)-Ibuprofen [33–38], denoted respectively (S)-NPX and (RS)-IBU.

4.1. The (S) - naproxen case

4.1.1. Step 1: PREOS solubility modeling and determination of k_{ij} parameters

According to PREOS presented in the first section, we have chosen to fit the (S)-NPX experimental solubility data set of Ting *et al.* [30] at 313.1 K, both with the Subcooled liquid and LK solid fugacity models ($LK^{original}$ and LK^{B3}), on a range of pressure from about 100 bar to 200 bar, standard work pressure in supercritical crystallization process. The original data set of Ting *et al.* [30] is reported in appendix, Table A.3.

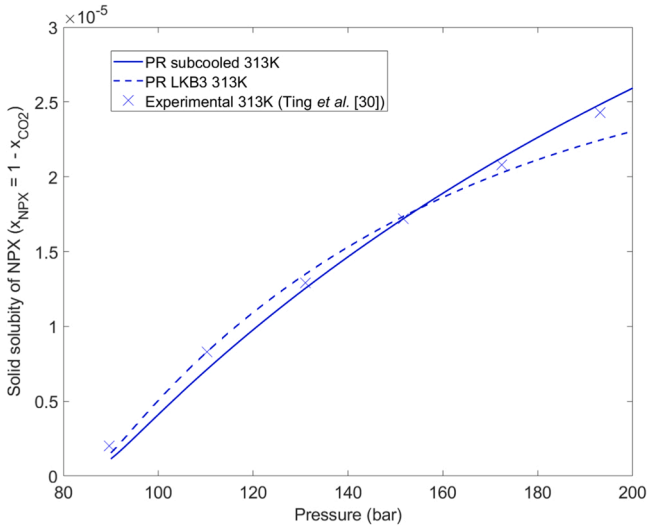

Fig. 4. (S)-NPX experimental and PREOS solubilities at 313 K.

The fitted PREOS k_{ij} parameters and the AARD(x_{NPX}) at 313.1 K are reported in Table 2:

The LK^{B3} model is the best to describe the solubility of (S)-NPX in supercritical CO_2 and the k_{ij} are quite similar to the PREOS k_{ij} of the Subcooled liquid model, while the $LK^{original}$ model leads to unaccurate predictions.

The solid solubilities are compared with experimental data for the Subcooled liquid and LK^{B3} modeling in Fig. 4:

4.1.2. Step 2: liquid-vapour equilibrium and the spinodal limits estimation

The knowledge of the PREOS k_{ij} has then been used to predict the liquid – vapour equilibrium and the spinodal limits of the {(S)-NPX + CO_2} mixtures. The (P, x_{CO2}) phase diagram at T = 313.1 K using the Subcooled liquid modeling, including the spinodal limits, is presented in Fig. 5a on a large scale and in Fig. 5b close to pure CO_2 (the LK^{B3} model leads to very similar results):

Several noteworthy observations have to be highlighted. First, PREOS predicts the existence and the composition of a liquid phase which would appear at sufficiently high molar (S)-NPX fractions in single phased supercritical {(S)-NPX + CO_2} mixtures when reaching the liquid dew line. For example, at a pressure of 150 bar, a liquid phase can appear when the (S)-NPX molar fraction is greater than 0.0004 ($x_{CO2} \approx 0.9996$, Fig. 5b) and the composition of the liquid phase is determined at the bubble point with $x_{CO2} \approx 0.37$ (Fig. 5a). Secondly, the upper part of the spinodal curve is "opened". Particularly, the upper spinodal curve has to be calculated in two steps (the liquid spinodal on the left and the vapour spinodal on the right) using different initial values of molar volume V_m. This is not due to numerical problem but it reveals that there is no upper spinodal curve at 313.1 K between approximatively 0.74 and 0.98 in CO_2 molar fraction. The particular shape of the spinodal curve in a (P, T) diagram has already been highlighted by Heidemann and Khalil [26], with an unconditionally unstable mixture for all the pressures above the pressure of the lowest vapour spinodal. An example is given in Fig. 6 at $x_{CO2} = 0.8$.

Furthermore, two domains of vapour metastability are highlighted in Fig. 5b. The first domain lies between the dew line and the solid – vapour equilibrium, where the vapour is metastable only with respect to solid – vapour separation, which means that in this zone nucleation will lead to pure solid particles. In the second domain with molar fractions of (S)-NPX higher than given by the dew line, the vapour is metastable with respect to solid – vapour separation and with respect to liquid – vapour separation, which means that in this zone nucleation will lead to pure solid particles and/or liquid droplets with compositions given by the bubble curve. From this point of view, the liquid – vapour equilibrium

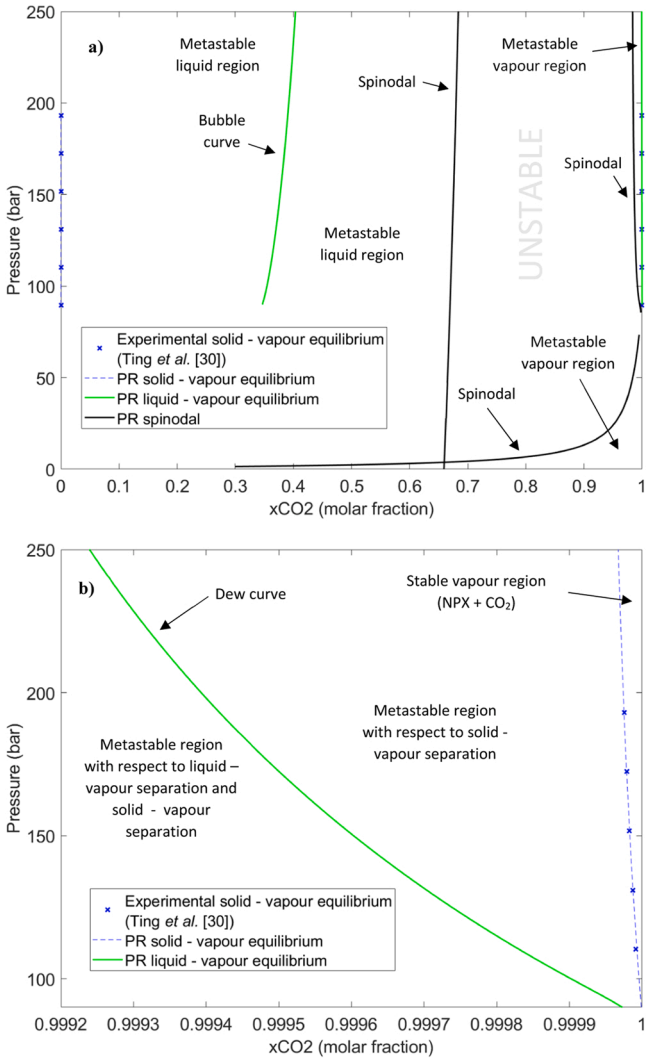

Fig. 5. a) {(S)-NPX + CO2} mixtures at 313.1 K, Subcooled liquid modeling, (P, xCO2) diagram; b) {(S)-NPX + CO2} mixtures at 313.1 K, Subcooled liquid modeling, (P, xCO2) diagram (detailed close to pure CO2). Blue color is used to describe the solid – vapour equilibrium, with the solid composition on the left side of the diagram in Fig. 5a (pure solid), and the vapour composition on the right side of the diagram in Fig. 5a and Fig. 5b. Green color is used to describe the liquid – vapour equilibrium, with the liquid composition on the left side of the diagram in Fig. 5a (bubble curve), and the vapour composition on the right side of the diagram in Fig. 5a and Fig. 5b (dew curve). Lastly, black color is used to describe the spinodal limits, with the liquid spinodal composition on the left of the diagram, and the vapour spinodal composition on the right and at the bottom in Fig. 5a.

can be qualified as a metastable equilibrium with respect to the solid – vapour equilibrium.

4.1.3. Step 3: estimation of supersaturation levels to reach stable/metastable/unstable states

To quantify and represent in a simple way the distances between the vapour spinodal limit, the metastable liquid – vapour equilibrium (the dew line) and the solid – vapour equilibrium, we can introduce the "molar supersaturation" S, simply defined as the ratio of the molar fraction of (S)-NPX in the vapour phase and the molar fraction of (S)-NPX in the vapour phase at the solid - vapour equilibrium, at given pressure and temperature:

$$S_{dew} = \left(\frac{x_{NPX,dew\ line}}{x_{NPX,solid-vapour\ equilibrium}} \right)_{T,P} \quad (38)$$

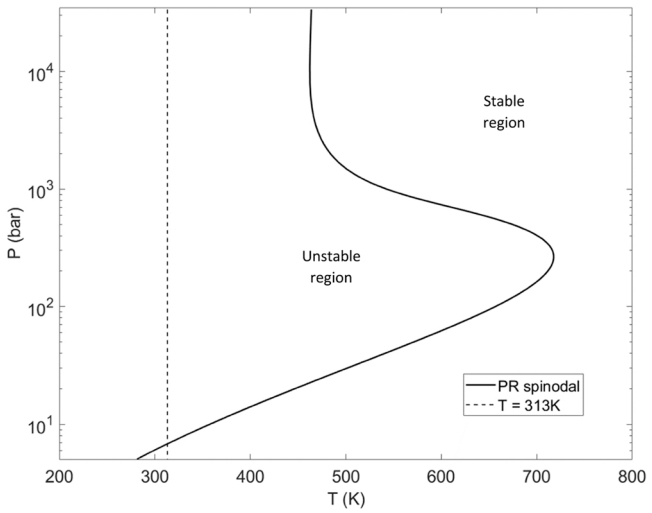

Fig. 6. Spinodal limits of a {(S)-NPX + CO2} mixture, $x_{CO2} = 0.8$, k_{ij}(313.1 K), (P, T) diagram.

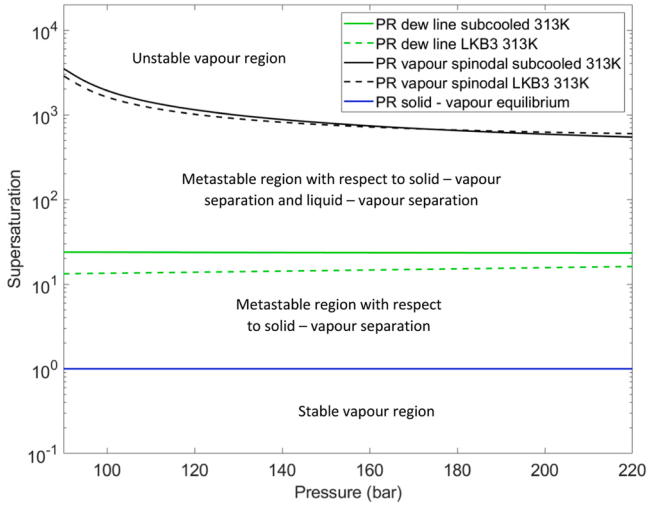

Fig. 7. (S)-NPX supersaturations at 313.1 K, (S, P) diagram.

$$S_{vapour\ spinodal} = \left(\frac{x_{NPX,vapour\ spinodal}}{x_{NPX,solid-vapour\ equilibrium}} \right)_{T,P} \quad (39)$$

This definition leads to S = 1 for the solid – vapour equilibrium. The results are presented in Fig. 7 for both Subcooled liquid and LK^{B3} calculations:

S ranges from about 10–25 (depending on the solid fugacity model) on this range of pressure at 313.1 K for the metastable liquid – vapour equilibrium, whereas supersaturation goes up to 800 – 4000 to reach the vapour spinodal limit. It means that while it may be possible to observe (S)-NPX liquid droplets before crystallization, it may be very difficult to observe a spinodal decomposition in {(S)-NPX + CO_2} mixtures at 313.1 K before crystallization on this range of pressure.

Table 3
PREOS kij and AARD on solubility for (RS)-IBU at 313.1 K.

Subcooled liquid method		Lee – Kesler equation	
k_{ij}	AARD (%)	k_{ij}	AARD (%)
0.07674	15.3	0.07859 (original) 0.00443 (B3)	8.9 (original) 18.7 (B3)

4.2. The (RS) - ibuprofen case

4.2.1. Step 1: PREOS solubility modeling and determination k_{ij} parameters

The data set of solubilities measured at 313 K by Charoenchaitrakool *et al.* [33] has been first selected for the determination of the interaction parameters k_{ij}, both with the Subcooled liquid and LK models ($LK^{original}$ and LK^{B3}). A second data set will be used (Martin [35]) in the discussion part to emphasise the possible appearance of solute liquid droplets before solid phase crystallization.

The original data sets of Charoenchaitrakool *et al.* [33] and Martin [35] are reported in appendix, Table A.4 and Table A.5 respectively.

The k_{ij} parameters and the AARD are reported in Table 3.

The $LK^{original}$ model is the best to describe the solubility of (RS)-IBU in supercritical CO_2 and the k_{ij} are quite similar to the k_{ij} of the Subcooled liquid model, while the LK^{B3} model leads to inconsistent results. The Subcooled liquid model leads to relatively unaccurate predictions. It may be explained by the choice of the (RS)-IBU physical properties (T_C, P_C, ω), estimated by a contribution group method leading to great variations, as reported by Kusnetzova *et al.* [36], and (T_m, ΔH_m), estimated by DSC measurements also subject to variations.

The solid solubilities are compared for the Subcooled liquid and $LK^{original}$ models in Fig. 8 in the pressure range of the study:

The two models seem to diverge considerably from each other above approximatively 180 bar.

4.2.2. Step 2: liquid-vapour equilibrium and the spinodal limits estimation

Both Subcooled liquid and $LK^{original}$ models lead to the same trends for the determination of the phase equilibria. We chose to plot only the "subcooled" model in Fig. 9.

We can note that, as for (S)-NPX, PREOS predicts the existence and the composition of a metastable liquid phase which would appear at sufficiently high molar IBU fractions in a single phased supercritical {CO_2 + (RS) - IBU} mixture, when reaching the dew line. But, compared with (S)-NPX, the metastable liquid phase is almost 2 times richer in CO_2, with $x_{CO2} \approx 0.7$.

By zooming close to pure CO_2, we can observe that both Subcooled liquid and $LK^{original}$ models predict that the solid – vapour and metastable liquid – vapour equilibria are very close together (Fig. 10a and Fig. 10b).

4.2.3. Step 3: estimation of supersaturation levels to reach stable/metastable/unstable states

The supersaturation of the vapour phase at the metastable liquid – vapour equilibrium (dew line) and at the spinodal vapour limit (Eqs. (38) and (39)) are given in Fig. 11 for both Subcooled liquid and LK^{B3}

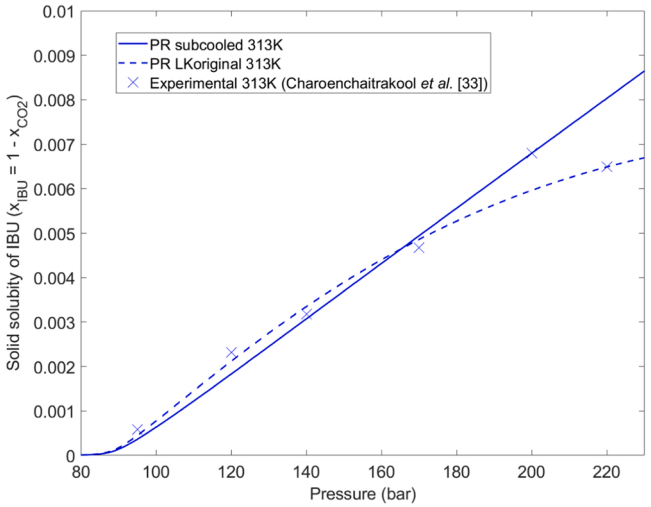

Fig. 8. (RS)-IBU experimental and PREOS solubilities at 313.1 K.

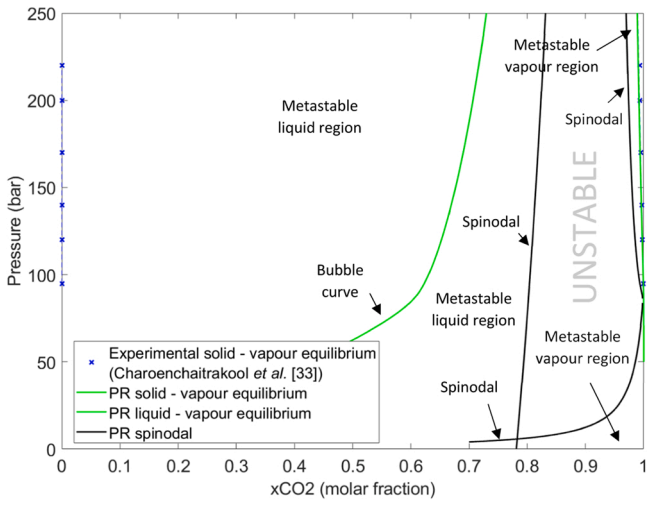

Fig. 9. {(RS)-IBU + CO2} mixtures at 313.1 K, Subcooled liquid modeling, (P, xCO2) diagram. Blue color is used to describe the solid – vapour equilibrium, with the solid composition on the left side of the diagram (pure solid), and the vapour composition on the right side. Green color is used to describe the liquid – vapour equilibrium, with the liquid composition on the left side of the diagram (bubble curve), and the vapour composition on the right side of the diagram (dew curve). Lastly, black color is used to describe the spinodal limits, with the liquid spinodal composition on the left of the diagram, and the vapour spinodal composition on the right and at the bottom.

calculations.

Both Subcooled liquid and $LK^{original}$ models lead to close supersaturations with $S \approx 1$ as expected to reach the dew line, whereas supersaturations goes up to 3 – 20 to reach the vapour spinodal limit. However, an important difference can be denoted concerning the metastable liquid – vapour equilibrium supersaturation. The two models do not predict the same trend according to pressure: the Subcooled liquid model predicts a decreasing supersaturation, with possibly a triple-point ($S = 1$) at higher pressure, whereas this is not the case with the $LK^{original}$ model, while increasing supersaturation.

4.3. Discussion

4.3.1. Comparison of the PREOS predictions for (S)-NPX and (RS)-IBU

The comparison of (S)-NPX and (RS)-IBU PREOS predicted behaviours leads to several interesting results that have to be highlighted. First, the two PREOS models predict the existence of a metastable liquid phase when reaching the dew line, with compositions strongly dependent on the API, and provide self-consistent predictions with the same order of magnitude for each API, concerning both the metastable liquid – vapour equilibria and the spinodal limits.

The supersaturation levels to reach the dew line and the spinodal vapour limit are very different for (S)-NPX on one hand, or (RS)-IBU at 313.1 K. Particularly, it seems that the metastable liquid phase and the spinodal decomposition would be more difficult to observe at 313.1 K in the case of (S)-NPX, with relatively high supersaturation, compared with (RS)-IBU.

Specifically concerning the metastable liquid phase, previous calculations showed that the supersaturation S to reach the dew line is remarkably almost constant on the studied pressure range at 313.1 K for (S)-NPX, and for (RS)-IBU to a lesser extent (Fig. 7 and Fig. 11). This fact can be demonstrated in a general framework starting from the equalities of the fugacities of the API in both liquid and vapour phases for the liquid – vapour equilibrium (Eq. (40), index LV), and in both solid and vapour phases when studying the solid - vapour equilibrium (Eq. (41), index SV):

$$\varphi^{V}_{API,LV}(T,P,\boldsymbol{x_{LV}})x^{V}_{API,LV}P = \varphi^{L}_{API,LV}(T,P,\boldsymbol{x_{LV}})x^{L}_{API,LV}P \quad (40)$$

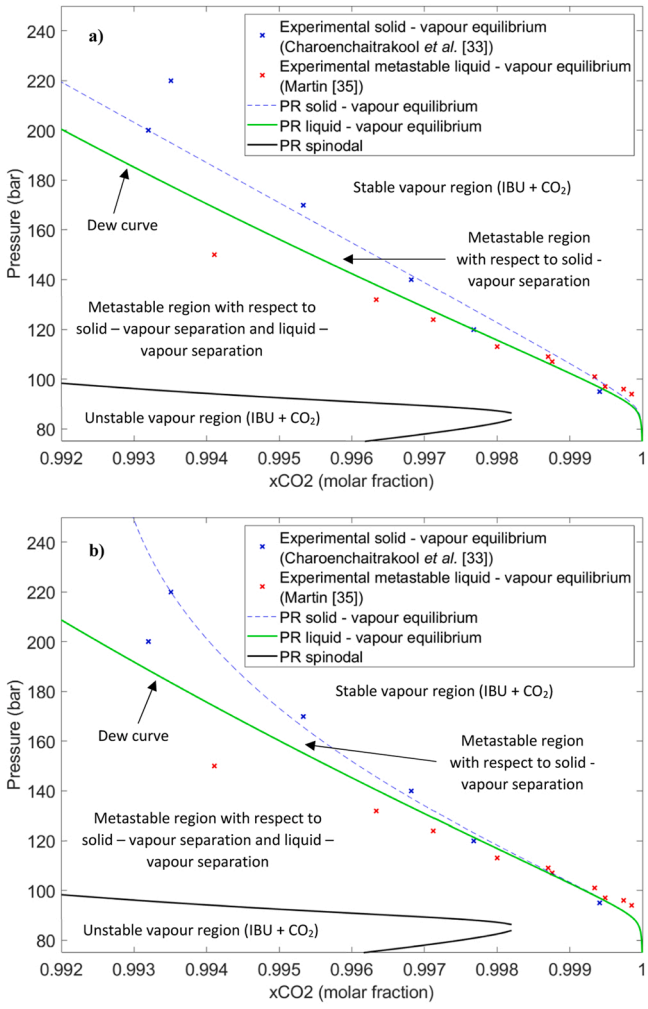

Fig. 10. a) {(RS)-IBU + CO_2} mixtures at 313.1 K, Subcooled liquid modeling, (P, x_{CO2}) diagram (detailed close to pure CO_2); b) {(RS)-IBU + CO_2} mixtures at 313.1 K, LKoriginal modeling, (P, xCO_2) diagram (detailed close to pure CO_2).

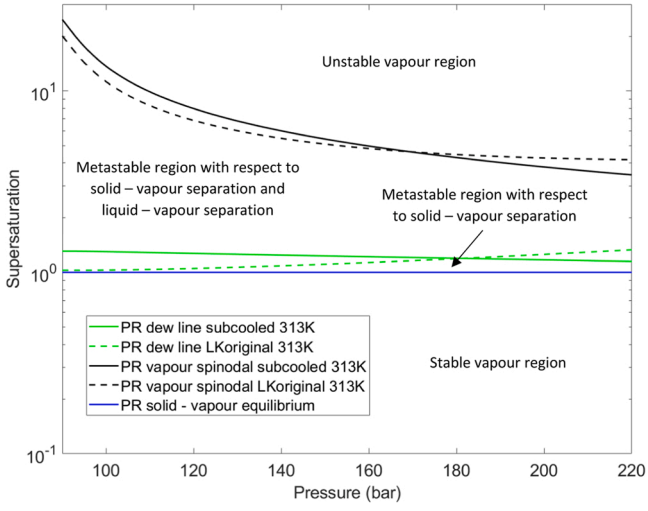

Fig. 11. (RS)-IBU supersaturations at 313.1 K, (S, P) diagram.

$$\varphi^{V}_{API,SV}(T,P,\boldsymbol{x_{SV}})x^{V}_{API,SV}P = f^{S}_{API,SV}(T,P) \tag{41}$$

Supersaturation to reach the dew line, introduced in Eq. (38), can be written as follow:

$$S_{dew} = \frac{x^{V}_{API,LV}}{x^{V}_{API,SV}} = \frac{\varphi^{V}_{API,SV}(T,P,\boldsymbol{x_{SV}})}{\varphi^{V}_{API,LV}(T,P,\boldsymbol{x_{LV}})}\frac{\varphi^{L}_{API,LV}(T,P,\boldsymbol{x_{LV}})x^{L}_{API,LV}}{f^{S}_{API,SV}(T,P)}P \tag{42}$$

By considering the Subcooled liquid model for the solid fugacity, Eq. (42) becomes:

$$S_{dew} = \frac{x^{V}_{API,LV}}{x^{V}_{API,SV}} = \left(\frac{\varphi^{V}_{API,SV}(T,P,\boldsymbol{x_{SV}})}{\varphi^{V}_{API,LV}(T,P,\boldsymbol{x_{LV}})}\right)\left(\frac{\varphi^{L}_{API,LV}(T,P,\boldsymbol{x_{LV}})}{\varphi^{Lpure}_{API}(T,P)}\right)x^{L}_{API,LV}\exp\left[\frac{\Delta H_{m,API}}{RT_{m,API}}\left(\frac{T_{m,API}}{T}-1\right)\right] \tag{43}$$

In the particular case of (S)-NPX, it can be demonstrated using PREOS calculations that the two fugacity coefficients vapour and liquid ratios in Eq. (43) are almost equal to 1. For the vapour ratio, this is due to the very close compositions of the vapour phases for both solid – vapour and liquid – vapour equilibria. For the liquid ratio, the fugacity of the liquid phase does not depend strongly on its composition for low CO_2 molar fraction. We can then obtain the following simple Eq. (44), valid for temperature below the normal melting point of (S)-NPX:

$$S_{dew} \approx x^{L}_{NPX,LV}\exp\left[\frac{\Delta H_{m,NPX}}{RT_{m,NPX}}\left(\frac{T_{m,NPX}}{T}-1\right)\right] \tag{44}$$

Furthermore, previous PREOS calculations (Fig. 5a) showed that the molar fraction of (S)-NPX in the liquid phase $x^{L}_{NPX,LV}$ is almost constant on the studied range of pressure, so that the supersaturation can be considered almost constant. Eq. (44) seems to give good approximations in the case of (S)-NPX: for example, at T = 313.1 K, P = 150 bar and $x^{L}_{NPX} \approx 0.62$ (Fig. 5a), Eq. (44) leads to S ≈ 21.5, close to the previously calculated value S ≈ 23.5 using full PR Subcooled liquid model.

Within the framework of this model, the normal melting properties of the API (normal melting temperature and melting enthalpy) and the working temperature will have a major impact on the distance between the solid – vapour and metastable liquid – vapour equilibria. In particular, working close to the normal melting temperature of the API will make it easier to observe the metastable liquid phase with supersaturation close to unity, as shown in our study with $T_{m,\,(RS)\text{–}IBU} = 354$ K vs $T_{m,\,(S)\text{–}NPX} = 458.8$ K for an operating temperature of 313.1 K.

The precise range of validity of Eq. (44) has to be studied, but it could be potentially useful to estimate the distance between the solid – vapour and metastable liquid – vapour equilibria for various compounds in supercritical CO_2 knowing only their experimental normal melting properties.

4.3.2. *Metastable liquid droplets of (RS) – IBU and experimental operating procedures*

Our PREOS calculations showed in previous parts that the dew line was very close to the solid – vapour equilibrium in the case of (RS)-IBU at 313.1 K with supersaturation close to unity. It indicates that (RS)-IBU would be a good candidate to experimentally test our framework with possible metastable liquid droplets formation observed before crystallization. For this purpose, the experimental (RS)-IBU solubility data of Charoenchaitrakool *et al.* [33] and Martin [35] at 313.1 K are both reported in Fig. 12.

The solubilities diverge at pressure higher than approximatively 120 bar, but most important is that Martin [35] reported that he observed liquid droplets on the whole range of pressure. It is then possible that Martin [35] measured a liquid solubility curve, whereas

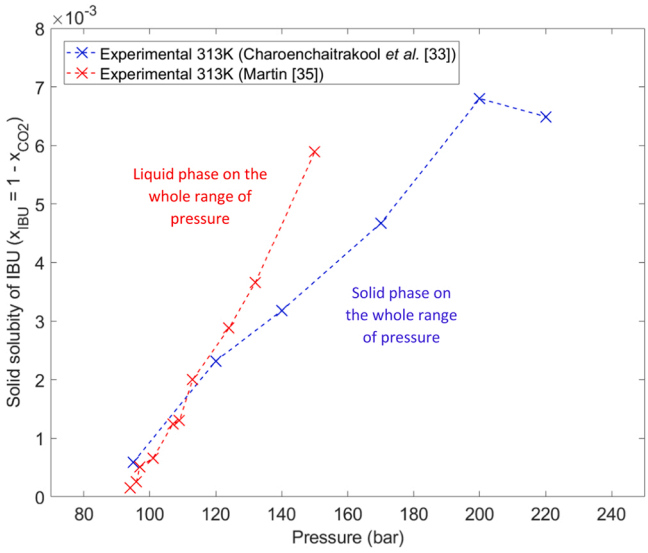

Fig. 12. (RS)-IBU experimental solubility curves at 313.1 K.

Charoenchaitrakool *et al.* [33] worked on solid phases.

The liquid solubility data of Martin [35] are plotted on Fig. 10a and Fig. 10b to compare with PREOS predictions. We can observe that the experimental liquid solubility data of Martin [35] follow the trend of the metastable dew line predicted by PREOS for both Subcooled liquid and $LK^{original}$ models, very close to the solid - vapour equilibrium of Charoenchaitrakool *et al.* [33].

Experimentally, it must be highlighted that the operating experimental procedures used by Charoenchaitrakool *et al.* [33] and Martin [35] are fundamentally different. Charoenchaitrakool *et al.* [33] worked in an equilibrium cell at given T and P, measuring the composition of the vapour phase coexisting with the solid phase, whereas Martin [35] is varying T and/or P in a view-cell at given global composition to observe phase appearance and locate solid – vapour equilibria or dew lines (more details about the operating procedures in references [33,35]). The procedure used by Martin [35] could sometimes induce a bias, with possible delayed phase transitions (vapour phase to solid phase for crystallization, or vapour phase to liquid phase for droplets formation), for systems with very low transformation kinetics.

To explain the droplets observations, Martin [35] assumed that there was an imbalance in the enantiomeric ratio of the studied (RS)-IBU solid samples, lowering their melting temperatures. Indeed, the normal melting temperature of enantiopure (R) or (S)-IBU is about 30 K lower than that of racemic (RS)-IBU and has been measured by Charoenchaitrakool *et al.* [33] at $T_m \approx 324.2$ K. Here, we proposed another interpretation, based on the highlighted previous elements. By considering the experimental procedure of Martin [35], the kinetical pathway seems here to play an important role, so it is possible that the solubility measured is that of the metastable liquid, since he directly observed the formation of the metastable liquid phase. This assumption is supported by the fact that Martin [35] also reported same behaviour at 308 K. When depressurising to reach the dew point, he observed initially the formation of liquid droplets, which become solid after 30 – 60 s. This may be the observation of a metastable liquid state leading to the formation of the solid, which could be qualified as a two-step nucleation process.

So, in our opinion, these comparisons between the (RS)-IBU solubility experimental data and observations of Charoenchaitrakool *et al.* [33] and Martin [35] on one hand, and the PREOS predictions on the other hand, support the fact that such a thermodynamical framework can help to better understand some experimental anomalies during supercritical crystallization processes.

Finally, to the best of our knowledge, metastable liquid – vapour

equilibrium highlighted in this paper has never been taken in account in classical supercritical crystallization processes such as RESS or SAS processes. We demonstrated by a thermodynamical evaluation that non classical nucleation could occur in some of our experimental configurations. We think that it could sometimes be of great importance because it could makes it possible to better understand and control amorphous particles production (by quenching for example the liquid droplets), or vary the crystal particle properties controling crystallization directly inside or outside the liquid droplets.

5. Conclusion

This study proposes a thermodynamical framework to study two-step nucleation in vapour supercritical conditions. It is based on the well-known Peng – Robinson Equation of State (PREOS) to describe the fluid phases and solid fugacity model. Two different solid fugacity models have been compared. The binary reference mixtures are studied at 40 °C, using experimental solid solubility data obtained from the literature, {(S)-naproxen + CO_2} and {(RS)-ibuprofen + CO_2}. Phase diagrams are presented in which stability / metastability and instability regions are highlighted, showing that PREOS predicts for both solid models the existence of a metastable liquid phase which could appear at moderate supersaturation. A simplified equation is presented and can be used to estimate such supersaturation by knowing only the API normal melting properties. The spinodal limits are also calculated and are reached at higher supersaturation. This work can provide keys to a better understanding of processes such as RESS or SAS to be able to target the production of amorphous or crystal organic materials in supercritical CO_2. For SAS applications, this work will be extended to ternary system.

CRediT authorship contribution statement

P. Guillou: Writing – review & editing, Writing – original draft, Software, Methodology, Investigation, Formal analysis, Conceptualization. **S. Marre**: Writing – review & editing, Supervision, Investigation, Conceptualization. **A. Erriguible:** Writing – review & editing, Supervision, Project administration, Methodology, Investigation, Funding acquisition, Conceptualization.

Declaration of Competing Interest

The authors declare that they have no known competing financial interests or personal relationships that could have appeared to influence the work reported in this paper.

Data Availability

Data will be made available on request.

Acknowledgement

We acknowledge the French National Research Agency for its support (ANR22-CE51–0023–01 - SUCRINE).

Appendix

Nomenclature	
A	Helmholtz free energy of a single phased mixture (J)
A_{excess}	excess part of the Helmoltz free energy of a single phased mixture (J)
a_i	PREOS energy parameter relatively to compound i ($J.m^3.mol^{-2}$)
A_{ideal}	ideal part of the Helmoltz free energy of a single phased mixture (J)
a_m	PREOS energy parameter ($J.m^3.mol^{-2}$)
b_i	PREOS volume parameter relatively to compound i ($m^3.mol^{-1}$)
b_m	PREOS volume parameter ($m^3.mol^{-1}$)
f_i^L	fugacity of compound i in a liquid phase (Pa)
f_i^S	fugacity of compound i in a solid phase (Pa)
f_i^V	fugacity of compound i in a vapour phase (Pa)
-	
I	identity matrix
k_{ij}	PREOS binary interaction parameter between compounds i and j (adimentional)
N	total molar quantity (mol)
$\mathbf{N}$	vector of molar quantities (mol) $\boldsymbol{N} = [N_1, N_2, \ldots, N_n \quad]$
$\overline{\mathbf{N}}$	vector of molar quantities at a fixed composition (mol) $\overline{\boldsymbol{N}} = [\overline{N_1}, \overline{N_2}, \ldots, \overline{N_n} \quad]$
N_i	molar quantity of compound i (mol) $N = \sum_i N_i$
$\overline{N_i}$	molar quantity of compound i at a fixed composition (mol) $N = \sum_i \overline{N_i}$
P	pressure (Pa)
P_0	triple-point pressure of the API (Pa)
P^0	standard pressure = 1 bar
P_c	critical pressure of a mixture (Pa)
$P_{c,i}$	critical pressure of compound i (Pa)
$P_{r,i}$	reduced pressure relatively to compound i (adimentional) $P_{r,i} = \frac{P}{P_{c,i}}$
$P_{sub,i}$	sublimation pressure of compound i (Pa)
R	ideal gas constant = 8.314 $J.mol^{-1}.K^{-1}$
T	temperature (K)
T_c	critical temperature of a mixture (K)
$T_{c,i}$	critical temperature of compound i (K)
$T_{m,i}$	normal melting temperature of compound i (K) at P_{atmos} = atmospheric pressure = 101325 Pa
$T_{r,i}$	reduced temperature relatively to compound i (adimentional) $T_{r,i} = \frac{T}{T_{c,i}}$
V	volume (m^3)
v_i^L	liquid molar volume of pure compound i ($m^3.mol^{-1}$)
v_i^S	solid molar volume of pure compound i ($m^3.mol^{-1}$)
V_m	molar volume ($m^3.mol^{-1}$)

(*continued on next page*)

(*continued*)

Nomenclature	
x_i	molar fraction of compound i in a single phased mixture (adimentional) $x_i = \frac{N_i}{N}$
Z	compressibility factor of a singled phased mixture (adimentional)
α_i	PREOS α(T) parameter relatively to compound i (adimentional)
$\Delta H_{m,i}$	normal melting enthalpy of compound i (J.mol^{-1}) at P_{atmos} = atmospheric pressure = 101325 Pa
$\boldsymbol{\varepsilon}$	vector of the substitution variables ε_i $\boldsymbol{\varepsilon} = [\varepsilon_1, \varepsilon_2, \ldots, \varepsilon_n \quad]$
ε_i	substitution variable to N_i in order to normalize the ideal part of Φ (J$^{1/2}$)
μ_i^0	standard chemical potential of compound i (J/mol) at standard pressure (P^0 = 1 bar)
$\Phi = \nabla_{\boldsymbol{N}}\nabla_{\boldsymbol{N}}A(T,V,\boldsymbol{N})$	part of the Hessian matrix of the Helmoltz free energy relatively to the molar quantities, so called "Hessian composition matrix"
φ_i^L	fugacity coefficient of compound i in a liquid phase (adimentional)
φ_i^S	fugacity coefficient of compound i in a solid phase (adimentional)
φ_i^V	fugacity coefficient of compound i in a vapour phase (adimentional)
ω_i	acentric factor of compound i (adimentional)
$\nabla_{V,\boldsymbol{N}}\nabla_{V,\boldsymbol{N}}A(T,V,\boldsymbol{N})$	Hessian matrix of the Helmoltz free energy at fixed (T, V, **N**)

Physical properties and experimental data

Table A.1
Physical properties of the compounds studied in this document

	M (g.mol^{-1})	T_C (K)	P_C (bar)	ω	10^6. V_i^S (m^3.mol^{-1})	$T_{m,i}$ (K)	$\Delta H_{m,i}$ (kJ.mol^{-1})
Methane	16.04[a]	190.56[a]	45.99[a]	0.01142[a]	-	-	-
Ethane	30.07[a]	305.32[a]	48.72[a]	0.0995[a]	-	-	-
Propane	44.10[a]	369.89[a]	42.51[a]	0.1521[a]	-	-	-
n-butane	58.12[a]	425.13[a]	37.96[a]	0.201[a]	-	-	-
n-heptane	100.20[a]	540.20[a]	27.36[a]	0.349[a]	-	-	-
Nitrogen	28.01[a]	126.19[a]	33.96[a]	0.0372[a]	-	-	-
CO_2	44.01[a]	304.1[a]	73.77[a]	0.22394[a]	-	-	-
(S) – Naproxen	230.26[a]	807[b]	24.52[b]	0.904[b]	179.0[b]	428.8[a]	34.2[a]
(RS) – Ibuprofen	206.28[a]	776.8[c]	21.3[c]	0.932[c]	185.8[d]	354[c]	23.68[c]

[a] NIST Webbook database
[b] Coimbra *et al.* [39]
[c] Martin [35]
[d] Uchida *et al.* [34]

Table A.2
Parameters of the Lee - Kesler equation (original and B3 sets)

Parameter	$LK^{original}$ Lee and Kesler [19]	LK^{B3} (Wang and Hsieh [20])
A_1	5.92714	5.92714
A_2	-6.09648	-6.09648
A_3	-1.28862	-1.28862
A_4	0.169347	0.169347
B_1	15.2518	15.2518
B_2	-15.6875	-15.6875
B_3	-13.4721	-10.9803
B_4	0.43577	0.43577

Table A.3
(S)-NPX experimental solubility data set of Ting et al. [30]

Pressure (bar)	Solubility of (S)-NPX at 313.1 K: (S)-NPX molar fraction in the vapour phase at solid – vapour equilibrium, Ting *et al.* [30], $10^5.x_{NPX}$
89.6	0.2
110.3	0.83
131.0	1.29
151.7	1.72
172.4	2.08
193.1	2.43

Table A.4
(RS)-IBU original experimental solubility data set of Charoenchaitrakool et al. [33]

Pressure (bar)	Solubility of racemic IBU at 313.1 K: (RS)-IBU molar fraction in the vapour phase at solid – vapour equilibrium, Charoenchaitrakool *et al.* [33], $10^3.x_{IBU}$
95	0.585
120	2.32
140	3.18
170	4.67
200	6.80
220	6.49

Table A.5
(RS)-IBU original experimental solubility data set of Martin [35]

Pressure (bar)	Solubility of racemic IBU at 313 K: (RS)-IBU molar fraction in the vapour phase at liquid – vapour equilibrium, Martin [35]: $10^3.x_{IBU}$
94	0.15
96	0.26
97	0.51
101	0.66
107	1.24
109	1.30
113	2.00
124	2.88
132	3.66
150	5.89

References

[1] H.D. Williams, N.L. Trevaskis, S.A. Charman, R.M. Shanker, W.N. Charman, C. W. Pouton, C.J.H. Porter, Strategies to address low drug solubility in discovery and development, Pharmacol. Rev. 65 (2013) 315–499, https://doi.org/10.1124/pr.112.005660.

[2] A. Schittny, J. Huwyler, M. Puchkov, Mechanisms of increased bioavailability through amorphous solid dispersions: a review, Drug Deliv. 27 (2020) 110–127, https://doi.org/10.1080/10717544.2019.1704940.

[3] A. Karagianni, K. Kachrimanis, I. Nikolakakis, Co-amorphous solid dispersions for solubility and absorption improvement of drugs: composition, preparation, characterization and formulations for oral delivery, Pharmaceutics 10 (2018) 98, https://doi.org/10.3390/pharmaceutics10030098.

[4] T. Jaouhari, F. Zhang, T. Tassaing, S. Fery-Forgues, C. Aymonier, S. Marre, A. Erriguible, Process intensification for the synthesis of ultra-small organic nanoparticles with supercritical CO2 in a microfluidic system, Chem. Eng. J. 397 (2020) 125333, https://doi.org/10.1016/j.cej.2020.125333.

[5] F. Zhang, S. Marre, A. Erriguible, Mixing intensification under turbulent conditions in a high pressure microreactor, Chem. Eng. J. 382 (2020) 122859, https://doi.org/10.1016/j.cej.2019.122859.

[6] P.G. Vekilov, Nucleation, Cryst. Growth Des. 10 (2010) 5007–5019, https://doi.org/10.1021/cg1011633.

[7] D. Gebauer, M. Kellermeier, J.D. Gale, L. Bergström, H. Cölfen, Pre-nucleation clusters as solute precursors in crystallisation, Chem. Soc. Rev. 43 (2014) 2348–2371, https://doi.org/10.1039/C3CS60451A.

[8] P.R. ten Wolde, D. Frenkel, Enhancement of protein crystal nucleation by critical density fluctuations, Science 277 (1997) 1975–1978, https://doi.org/10.1126/science.277.5334.1975.

[9] H. Fu, X. Gao, X. Zhang, L. Ling, Recent advances in nonclassical crystallization: fundamentals, applications, and challenges, Cryst. Growth Des. 22 (2022) 1476–1499, https://doi.org/10.1021/acs.cgd.1c01084.

[10] S. Xu, H. Zhang, B. Qiao, Y. Wang, Review of liquid–liquid phase separation in crystallization: from fundamentals to application, Cryst. Growth Des. 21 (2021) 7306–7325, https://doi.org/10.1021/acs.cgd.0c01376.

[11] E. Wiedenbeck, M. Kovermann, D. Gebauer, H. Cölfen, Liquid metastable precursors of ibuprofen as aqueous nucleation intermediates, Angew. Chem. Int. Ed. 58 (2019) 19103–19109, https://doi.org/10.1002/anie.201910986.

[12] Z. Zhang, R. Bi, J.-F. Audibert, W. Wang, S.Y. Park, A. Spasojević-de Biré, R. B. Pansu, Thermodynamics of oiling-out in antisolvent crystallization. I. extrapolation of ternary phase diagram from solubility to instability, Cryst. Growth Des. 24 (2024) 224–237, https://doi.org/10.1021/acs.cgd.3c00916.

[13] D.-Y. Peng, D.B. Robinson, A new two-constant equation of state, Ind. Eng. Chem. Fundam. 15 (1976) 59–64, https://doi.org/10.1021/i160057a011.

[14] J. De Swaan Arons, G.A.M. Diepen, Thermodynamic study of melting equilibria under pressure of a supercritical gas, Recl. Trav. Chim. Pays-Bas 82 (1963) 249–256, https://doi.org/10.1002/recl.19630820308.

[15] J.M. Prausnitz, R.N. Lichtenthaler, E. Gomes de Azevedo, Molecular Thermodynamics of Flui-Phase Equilibria 3rd Edition, Prentice Hall International Series In the Physical and Chemical Engineering Sciences, 1998.

[16] I. Kikic, M. Lora, A. Bertucco, A Thermodynamic Analysis of Three-Phase Equilibria in Binary and Ternary Systems for Applications in Rapid Expansion of a Supercritical Solution (RESS), Particles from Gas-Saturated Solutions (PGSS), and Supercritical Antisolvent (SAS), (n.d.) 9.

[17] M. Seiler, J. Groß, B. Bungert, G. Sadowski, W. Arlt, Modeling of solid/fluid phase equilibria in multicomponent systems at high pressure, Chem. Eng. Technol. 24 (2001) 607–612, https://doi.org/10.1002/1521-4125(200106)24:6<607::AID-CEAT607>3.0.CO;2-T.

[18] J.W. Tester, M. Modell, Thermodynamics and Its Applications 3rd Edition, Prentice Hall International Series In the Physical and Chemical Engineering Sciences, 1997.

[19] B.I. Lee, M.G. Kesler, A generalized thermodynamic correlation based on three-parameter corresponding states, Aiche J. 21 (1975) 510–527, https://doi.org/10.1002/aic.690210313.

[20] H.-W. Wang, C.-M. Hsieh, Prediction of solid solute solubility in supercritical carbon dioxide from PSRK EOS with only input of molecular structure, J. Supercrit. Fluids 180 (2022) 105446, https://doi.org/10.1016/j.supflu.2021.105446.

[21] Á. Martín, M.D. Bermejo, F.A. Mato, M.J. Cocero, Teaching advanced equations of state in applied thermodynamics courses using open source programs, e114–e121, Educ. Chem. Eng. 6 (2011), https://doi.org/10.1016/j.ece.2011.08.003.

[22] S.M. Walas, Phase Equilibria in Chemical Engineering, Butterworth-Heinemann, 1985.

[23] A.K. Gupta, P. Raj Bishnoi, N. Kalogerakis, A method for the simultaneous phase equilibria and stability calculations for multiphase reacting and non-reacting systems, Fluid Ph. Equilibria 63 (1991) 65–89, https://doi.org/10.1016/0378-3812(91)80021-M.

[24] J.W. Cahn, J.E. Hilliard, Free energy of a nonuniform system. I. interfacial free energy, J. Chem. Phys. (1958).

[25] J.W. Cahn, J.E. Hilliard, Free energy of a nonuniform system. III. Nucleation in a two-component incompressible fluid, J. Chem. Phys. (1959).

[26] R.A. Heidemann, A.M. Khalil, The calculation of critical points, Aiche J. 26 (1980) 769–779, https://doi.org/10.1002/aic.690260510.

[27] P. Aursand, M.Aa Gjennestad, E. Aursand, M. Hammer, Ø. Wilhelmsen, The spinodal of single- and multi-component fluids and its role in the development of modern equations of state, Fluid Ph. Equilibria 436 (2017) 98–112, https://doi.org/10.1016/j.fluid.2016.12.018.

[28] M.L. Michelsen, Calculation of critical points and phase boundaries in the critical region, Fluid Ph. Equilibria 16 (1984) 57–76, https://doi.org/10.1016/0378-3812(84)85021-9.

[29] M. Türk, Particle synthesis by rapid expansion of supercritical solutions (RESS): current state, further perspectives and needs, J. Aerosol Sci. 161 (2022) 105950, https://doi.org/10.1016/j.jaerosci.2021.105950.

[30] S.S.T. Ting, D.L. Tomasko, N.R. Foster, S.J. Macnaughton, Solubility of naproxen in supercritical carbon dioxide with and without cosolvents, Ind. Eng. Chem. Res. 32 (1993) 1471–1481, https://doi.org/10.1021/ie00019a022.

[31] M. Türk, T. Kraska, Experimental and theoretical investigation of the phase behavior of naproxen in supercritical CO $_2$, J. Chem. 54 (2009) 1592–1597, https://doi.org/10.1021/je800920d.

[32] A.P. Kloc, A. Danzer, G. Sadowski, Solubility of naproxen and indomethacin in supercritical carbon dioxide/ethyl acetate mixtures, J. Supercrit. Fluids 200 (2023) 105990, https://doi.org/10.1016/j.supflu.2023.105990.

[33] M. Charoenchaitrakool, F. Dehghani, N.R. Foster, H.K. Chan, Micronization by rapid expansion of supercritical solutions to enhance the dissolution rates of poorly water-soluble pharmaceuticals, Ind. Eng. Chem. Res. 39 (2000) 4794–4802, https://doi.org/10.1021/ie000151a.
[34] H. Uchida, M. Yoshida, Y. Kojima, Y. Yamazoe, M. Matsuoka, Measurement and correlation of the solid−liquid−gas equilibria for the carbon dioxide + *S* -(+)-ibuprofen and carbon dioxide + *RS* -(±)-ibuprofen systems, J. Chem. Eng. Data 50 (2005) 11–15, https://doi.org/10.1021/je034228o.
[35] Á. Martín, Precipitation Processes with Supercritical Carbon Dioxide: Mathematical Modeling and Experimental Validation, PhD manuscript, 2005.
[36] I.V. Kuznetsova, I.I. Gilmutdinov, I.M. Gilmutdinov, A.A. Mukhamadiev, A. N. Sabirzyanov, Solubility of ibuprofen in supercritical carbon dioxide, Russ. J. Phys. Chem. B 7 (2013) 814–819, https://doi.org/10.1134/S1990793113070105.
[37] M. Ardjmand, M. Mirzajanzadeh, F. Zabihi, Measurement and correlation of solid drugs solubility in supercritical systems, Chin. J. Chem. Eng. 22 (2014) 549–558, https://doi.org/10.1016/S1004-9541(14)60073-2.
[38] N.S. Ardestani, N.Y. Majd, M. Amani, Experimental measurement and thermodynamic modeling of Capecitabine (an Anticancer Drug) solubility in supercritical carbon dioxide in a ternary system: effect of different cosolvents, J. Chem. Eng. Data 65 (2020) 4762–4779, https://doi.org/10.1021/acs.jced.0c00183.
[39] P. Coimbra, C.M.M. Duarte, H.C. de Sousa, Cubic equation-of-state correlation of the solubility of some anti-inflammatory drugs in supercritical carbon dioxide, Fluid Ph. Equilibria 239 (2006) 188–199, https://doi.org/10.1016/j.fluid.2005.11.028.